Journal of Power Sources 251 (2014) 269–278

Contents lists available at ScienceDirect

Journal of Power Sources

journal homepage: www.elsevier.com/locate/jpowsour

Understanding the gas diffusion layer in proton exchange membrane fuel cells. I. How its structural characteristics affect diffusion and performance

Jason M. Morgan [a,b], Ravindra Datta [b,*]

[a] AvCarb Material Solutions, 2 Industrial Ave, Lowell, MA 01851, USA
[b] Fuel Cell Center, Department of Chemical Engineering, Worcester Polytechnic Institute, Worcester, MA 01609, USA

HIGHLIGHTS

- We provide a comprehensive discussion of GDL & MPL structural characteristics & how they are measured experimentally.
- We further examine the impact of these characteristics on transport & performance in proton exchange membrane fuel cells.
- Correlation between the effective diffusivity & the limiting current density is provided.
- The impact of the MPL structure on cell performance under wet as well as dry conditions is discussed.

ARTICLE INFO

Article history:
Received 22 June 2013
Received in revised form
19 September 2013
Accepted 21 September 2013
Available online 22 November 2013

Keywords:
PEM fuel cell
Gas diffusion layer (GDL)
Microporous layer (MPL)
GDL pore structure
GDL effective diffusivity
Limiting current density

ABSTRACT

The proton exchange membrane fuel cell (PEMFC) has a significant potential in transportation, backup, and portable power applications, although there still are remaining technical and cost challenges. A key current goal is improving the performance while reducing the cost of the gas diffusion layer (GDL). Designing a commercial GDL, however, is far more complex than simply making a porous, sturdy, conductive layer, because of the trade-offs among performance, manufacturability, and cost. An improved understanding of its multifarious functions in the fuel cell can help attain this goal. Here, we identify 11 key characteristic parameters of the GDL and their significance to its performance. We begin a discussion of some of these parameters in this paper, specifically those related to the structure of the GDL substrate and the microporous layer (MPL), how these are measured experimentally *ex-situ*, how they influence fuel cell performance, and how they can be altered via the manufacturing process. In particular, we investigate the correlation between *ex-situ* measured effective diffusivity of water vapor and *in-situ* performance and limiting current density in a PEM fuel cell. Further, we examine the effect of adding multiple MPLs, MPL loading, and MPL particle size on cell performance under both wet and dry operating conditions.

1. Introduction

Polymer electrolyte membrane (PEM) fuel cells are poised for transportation, backup power, and portable power applications [1]. They have many advantages including low operating temperature, quick starting time, high efficiency, low weight, and simple design. Despite these advantages, however, modern PEMFCs face many challenges before fully realizing their commercial potential. These include high cost, inadequate durability, hydrogen storage and distribution issues, and water management difficulties.

The cost breakdown of PEMFCs has been analyzed both by the Department of Energy (DOE) [2] and in the literature [3]. It has been concluded that there needs to be a significant reduction in both the capital (high-volume, low-cost production capability) and operational (improved stack efficiency) costs before PEMFCs can be fully commercialized. The life of a PEM fuel cell is limited by: 1) membrane durability, 2) catalyst durability, and 3) that of the balance of plant (BOP) components. Many investigators have examined the issue of membrane durability, e.g., the impact of side chain degradation by hydroxyl radicals [4], performance loss due to chemical and electrochemical degradation [5–7], and with the mechanisms of membrane degradation [8–10]. Others have focused on catalyst durability, specifically Pt migration [11–13], carbon support corrosion [14,15] and catalyst poisoning [16–18]. Much work has also been

* Corresponding author. Tel.: +1 508 831 6036.
E-mail address: rdatta@wpi.edu (R. Datta).

0378-7753/$ – see front matter © 2013 Published by Elsevier B.V.
http://dx.doi.org/10.1016/j.jpowsour.2013.09.090

done to investigate the BOP components for PEMFCs, namely, air blowers [19], heat exchangers [20,21], humidifiers [22–24] and power converters [25,26]. Our effort is focused on the often-neglected gas diffusion layer (GDL), its experimental and theoretical characterization, and issues related to its design, cost, and manufacturability.

The GDL is comprised of a highly porous woven carbon fabric, or a carbon fiber paper, that is treated with PTFE (Teflon) to make it hydrophobic, and then coated with a microporous layer (MPL) to form a 2-layer graded porous structure, as shown schematically in Fig. 1. The GDL is characterized by the following five key features [27], each of which requires specific, sometimes competing, GDL properties for desired performance:

1) *Reactant permeability*: This should be as high as possible to ensure an adequate supply of reactants (O_2/H_2), especially oxygen from air, to the catalyst layer so that the performance is limited by electrode kinetics, not by reactant transport. This requires the GDL to be macroporous and largely free of liquid water.
2) *Product permeability*: This should be high to remove water to the flow field effectively and prevent it from building up at the cathode catalyst layer (CCL), thereby blocking the reactant access to the catalyst, and. On the other hand, it should not be so high as to lead to membrane drying, which would reduce the proton conductivity of the membrane [28].
3) *Electrical conductivity*: This should be as high as possible to minimize Ohmic losses by effectively conducting electrons between the catalyst layer and the current collectors via the bipolar plate. However, it is reduced by increased porosity and PTFE content of the GDL, necessary for high reactant and product permeabilities.
4) *Thermal conductivity*: This should be high to effectively remove the heat from the membrane electrode assembly (MEA), where it is produced, to the bipolar plates, where cooling is available. The heat effects are mainly associated the cathode reaction, the Ohmic losses in the membrane, and water evaporation/condensation.
5) *Mechanical support*: The GDL must provide robust mechanical support to protect the membrane and catalyst layers from damage during assembly, while maintaining good interfacial contact among the MEA layers, to prevent damage from any pressure differentials across the MEA, and to avoid its deflection into the flow field channels during cell compression.

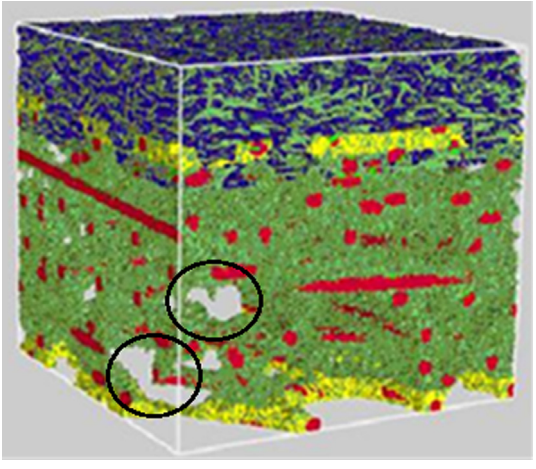

Fig. 1. 3-D rendering of GDL structure with carbon fiber in red, fill matrix in green, PTFE loading in yellow, MPL structure in blue, and some large pores circled. Made with GeoDict® software, and provided by Ballard Power Systems. (For interpretation of the references to color in this figure legend, the reader is referred to the web version of this article.)

The reactant permeability of the GDL, typically characterized by the effective oxygen diffusivity of the cathode GDL, usually determines the limiting current density, and is dependent on the pore structure and the thickness of the GDL as well as the saturation level, or water loading. The effective diffusivity is a function of the porosity, tortuosity, and the mean pore radius of the GDL [29–31], as discussed further below. More recently, efforts have also been made to relate it to other microstructural properties, such as pore shape, orientation, and connectivity [32,33]. Similarly, the product permeability of the GDL is controlled by its pores structure, thickness, as well as the PTFE content.

In addition, the transport properties of a GDL are greatly influenced by the MPL design (Fig. 1). Although, the GDL is often treated as a homogenous material, in reality the GDL substrate and MPL are separate, distinct layers. For clarity, thus, here we will refer to the carbon paper base layer without any MPL coating as simply the "substrate", while "GDL" implies the composite of the substrate plus the MPL. Further, although the substrate can be woven carbon cloth or a carbon fiber paper, the focus in this work is exclusively on the carbon fiber paper, since the woven fabrics are significantly more expensive than their paper counterparts, due to the higher amounts of expensive carbon fiber. This cost difference can be as much as ten-fold at high volume production, which is prohibitive to fuel cell commercialization.

Significant efforts have been made to examine the influence of the presence of an MPL [34–37], the optimization of the MPL thickness and composition [38–40], and the effect of critical MPL properties including pore size distribution, porosity, and hydrophobicity [41–43]. Some recent publications [44,45] provide an excellent review of experimental characterization of the *ex-situ* electrical, thermal, and mechanical properties of the GDL, so these are not the focus in this paper.

A key characteristic of the transport performance of a GDL is measuring *in-situ* the limiting current density of a fuel cell, at which the cell voltage drops to zero owing to mass transportation limitations, typically in the cathode GDL. Mathematical models have been developed for the limiting current density in terms of transport properties of the GDL [46–49]. The limiting current density, of course, affects the performance at lower currents as well and is, thus, critical. The development of GDLs with higher wet limiting current densities could allow for smaller, more energy efficient fuel cells with lower overall costs.

Despite significant progress in recent years, the further advancement of PEM fuel cells is limited in part by the lack of a good understanding of how the performance of a GDL is correlated to its structure and design. While much effort has been spent on optimizing GDL properties for specific applications, there has been little effort devoted to understanding how the demands on the GDL change with application, and how those demands can be met by altering the GDL design. Here, we focus on the structural properties of the GDL and MPL, describing how they are measured experimentally, and exploring how they influence fuel cell performance.

A total of 11 *ex-situ* GDL characteristics were identified that influence GDL performance, and are listed in Table 1 in order of their perceived importance. Some of these, i.e., those related to the GDL and MPL structure and design are discussed below in detail including why they are important, how they can be measured experimentally, and how they can be altered in the GDL manufacture. Other characteristics listed in Table 1 are left for discussion in future publications. All the GDLs used in this work were fabricated using a commercial low-cost, high-volume production process at AvCarb® Material Solutions in Lowell, MA, USA.

Table 1
Critical GDL characteristics and their relative significance to its performance.

GDL property	Reason	Importance (1–10)
Effective diffusivity	Critical for water management properties	10
GDL thickness	Critical for MEA sealing and cell compression uniformity	9
Number of MPLs	Critical for controlling pore structure in the GDL	8
MPL loading & particle size	Controls pore structure at the GDL/CL interface	7
MPL particle type	Impacts adhesion, water transport, and thermal management at the interface	7
Surface roughness	Impacts durability of the membrane and water management	6
PTFE content (GDL/MPL)	Significant impact on water management, electrical & thermal resistance	5
GDL permeability	Related to water management, flow sharing, etc.	5
Basis weight	Impacts GDL structure, durability, and performance	4
Tensile strength	Necessary for appropriate material handling (continuous processing)	4
Flexural stiffness	Related to deflection of GDL into flow channels	3

2. GDL physical structure

The modern, low-cost, GDL (Fig. 1) is comprised of a graphitized carbon fiber substrate that is saturated with a fill matrix composed of a binder material, carbon/graphite particles and viscosity agents. This is treated with PTFE to impart appropriate hydrophobicity level to it, and coated with an MPL to provide a graded pore structure to the GDL. The electrical and thermal properties of the substrate are dominated by the carbon fiber content and fill matrix, while the overall GDL properties are also influenced by the PTFE content of the substrate and the MPL thickness and composition. The mechanical properties are dominated by the thickness and the composition of the substrate, the manufacturing process conditions, the PTFE content in the substrate and the MPL, and the MPL composition.

The GDL physical structure is characterized by the following *ex-situ* properties: thickness, compressibility, porosity, pore size, and effective diffusion length. Understanding the direct impact of these properties on fuel cell performance, however, can be difficult because the *in-situ* performance is highly dependent on the condition of the GDL inside the fuel cell stack. Thus, a GDL under low compression has a significantly different thickness, porosity, and electrical/thermal conductivity than a GDL under high compression. These *ex-situ* properties are, thus, measured under "standard" conditions, that can be significantly different from those the GDL would experience inside the fuel cell stack.

2.1. GDL thickness and compressibility

The uniformity of compressed GDL thickness is of paramount importance to ensure proper sealing of the membrane electrode assembly (MEA) and to prevent leaking in the fuel cell stack. If the variation in the GDL thickness at the compressed load is more than 10–20 μm, then the MEAs might not seal properly, leading to leaks and cells with low performance, requiring expensive stack rebuilding. In general, a more compressible GDL may be able to handle thickness variations better by allowing thickness to be controlled by adjusting the compressive load during MEA fabrication, but overly compressible GDLs also tend to partially fill the flow field channels under compression, blocking flow and increasing the pressure drop.

When designing a GDL for a specific application, it is important to remember that thicker GDLs will provide better protection for the membrane, preventing damage during compression, and will generally have a higher total porosity due to reduced density. Thicker GDLs, however, have longer diffusion path lengths, tend to flood more easily, provide more thermal and electrical resistance than thinner GDLs [50], and typically cost more due to increased carbon fiber content. There can be as much as a 10% difference in cost for a 50% increase in thickness, but it should be noted that very thin materials (<100 microns) become more difficult to handle during production, which can thus increase costs due to reduced production yields. The optimal GDL thickness is very much dependent on the cell design and operating conditions, involving trade-offs among performance, durability, and cost. In general, for cells designed to operate at high current densities and wet conditions, the optimal GDL will be as thin as possible under compressed load. For cells designed for lower operating current densities or dry/self-humidified systems, thicker GDLs will help to better control the water content and improve performance over thinner GDL designs. The thickness of the GDL can be altered by adjusting the amount of fiber content in the base paper, altering the fill matrix that is added to the base carbon fiber structure, or modifying the MPL composition or thickness.

Measuring the GDL thickness may seem like a rather simple task, but issues can arise if precautions are not taken. The thickness should be measured at a nominal pressure (typically, 1–10 psi) as well as at a compressed load that will be experienced in the cell (typically, 100–350 psi). The thickness can be measured experimentally with a set of displacement probes used in conjunction with a load cell (e.g., Instron), as shown in Fig. 2. The pressure is applied slowly and evenly over an area of at least 15 cm^2 to prevent uneven compression on the surface of the GDL and each sample is measured multiple times to ensure accuracy. The surface of the displacement probes is cleaned to remove any debris/residue after testing, especially if the tested GDL has been coated with an MPL as particles may stick to the surface and influence subsequent readings. This is typically done in conjunction with compressibility measurements as described in the literature [45].

2.2. GDL pore structure

The pore volume and mean pore radius are typically measured via Intrusion Porosimetry, which involves injecting a non-wetting fluid (typically mercury) into the GDL at increasing pressures, and recording the intrusion volume under quasi-equilibrium

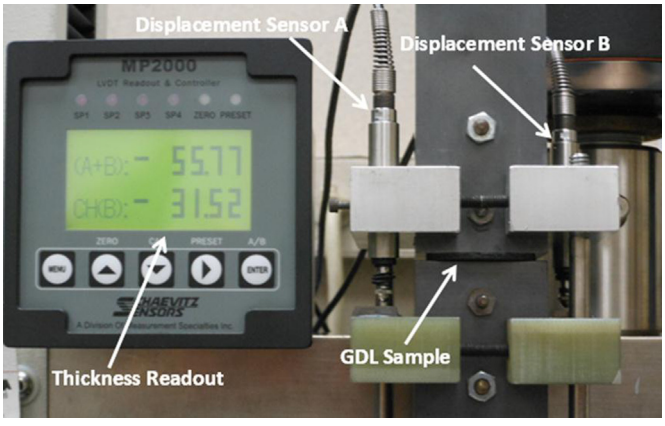

Fig. 2. Image of a GDL thickness measurement device utilizing two displacement sensors.

conditions. These data are then translated via the Kelvin Equation into the intrusion volume vs. pore size. Fig. 3 shows mercury intrusion porosimetry results for two GDL designs that are of similar construction, but different total thickness. The mean pore size can then be estimated along with pore volume and porosity. Although there is some concern over pore deformation due to the extremely high pressures that can be required for intrusion porosimetry, it is generally accepted as the standard technique for characterizing the pore structure.

The pore volume and mean pore radius of a GDL sample can be different for similar GDL designs with different thicknesses because of the inherent anisotropic structure (Fig. 1). As can be seen in Table 2, the thicker GDL has higher total pore volume and larger mean pore radius than the thinner material, although specific area is higher in the thinner GDL.

Wetting fluids (e.g., water/octane) could be similarly used to characterize only the hydrophobic pores of the GDL [51]. This is based on the assumption that any hydrophilic pores are immediately saturated by the wetting liquid, so that any increase in volume with applied pressure forces the liquid into hydrophobic pores only. This analysis can be compared to standard analysis with a non-wetting fluid, which measures all the pores, to determine the fraction of hydrophilic pores in the GDL.

The pore structure of the GDL (Fig. 1) can be modified by adjusting the carbon fiber content or the fill matrix in the substrate, altering the PTFE content in either the substrate or the MPL, adjusting the GDL manufacturing process (line speeds, heat treatment conditions, etc.) or altering the number of MPLs and their composition. It is, thus, possible to manufacture GDLs with a wide range of pore structures, size or shape, which can enhance performance under a given set of operating conditions.

3. GDL pore structure and transport properties

The gas-phase effective oxygen diffusivity of the GDL is the single most important property of the GDL for low temperature PEM fuel cells, as it determines the GDL transport controlled limiting current density of the cathode, given by

$$i_{C,L} = \frac{4F}{RT}\left(\frac{D^e_{O_2}}{L_D}\right)p_{O_2} \tag{1}$$

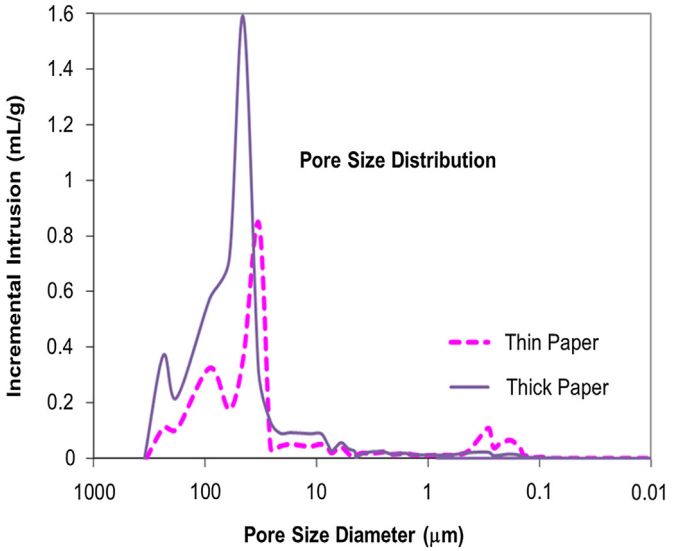

Fig. 3. Comparison of pore size distribution for thick and thin paper GDLs.

Table 2
A comparison of intrusion properties of thick vs. thin GDLs.

Property	Thick paper	Thin paper
Total intrusion volume (mL g^{-1})	4.9	2.9
Total pore area (m^2 g^{-1})	4.1	9.3
Median pore diameter (μm)	54	39
Porosity (%)	88	83

where F is the Faraday's constant, L_D is the GDL thickness, $D^e_{O_2}$ is the effective diffusivity of oxygen in the GDL, and p_{O_2} is the oxygen partial pressure in the cathode chamber, which can be different from the feed partial pressure, depending on feed flow rate and current density.

It has been shown in our previous work [49] that the dusty-gas model (DGM) can be used to model the effective gas-phase diffusivity of a gaseous species in the GDL. The dusty-gas model involves three DGM structural parameters characterizing the porous medium [49]; namely, K_0 is the DGM parameter for Knudsen diffusion, K_1, the DGM parameter for ordinary diffusion, and B_0, the d'Arcy permeability. These DGM parameters, in turn, may be estimated from the three more common structural properties, namely, the porosity (ε), the tortuosity (τ) and the mean pore radius (a), via

$$K_0 = \frac{\varepsilon}{\tau}\left(\frac{2}{3}a\right) \tag{2}$$

$$K_1 = \frac{\varepsilon}{\tau} \tag{3}$$

$$B_0 = \frac{\varepsilon}{\tau}\left(\frac{a^2}{8}\right) \tag{4}$$

Further, of course, all of these parameters, namely, ε, τ, and a, *in-situ* are strongly affected by the water loading in the GDL, q_W [52], also called saturation, S, in the fuel cell literature [53], i.e., the fractional pore volume occupied by water, which is clearly a function of the relative humidity (RH) in the fuel cell. Thus, from its definition

$$\frac{\varepsilon}{\varepsilon^0} = (1 - q_W) \tag{5}$$

where ε^0 is the dry porosity of the GDL (the superscript 0 represents dry). Further, Datta and Rinker [52] have provided correlations for the ratio of wet to dry tortuosity

$$\frac{\tau}{\tau^0} = \left(\frac{\varepsilon^0}{\varepsilon}\right)^{\alpha} = (1 - q_W)^{-\alpha} \tag{6}$$

where, e.g., $\alpha = 0.5$ corresponds to the Bruggeman correlation, while $\alpha = 1$ corresponds to the so-called random-pore model. The Bruggeman correlation, although commonly used in the fuel cell literature, has been shown to drastically underestimate the tortuosity factor of a GDL [54]. There are other models available in the literature that use different correlations between porosity and tortuosity [55,56], although it is not clear that any of these correlations are more accurate for GDLs, which are macroporous. Hwang and Webber [53] found that for GDLs, a better correlation is obtained with $\alpha \geq 2$.

Another reason for the difficulty in predicting the tortuosity factor of the GDL becomes clear when one more closely examines its structure, a 3-D rendering of which is shown in Fig. 1. It is clear from this image that the GDL is quite heterogeneous in both structure and composition. Further, some of the large pores do not

go completely through the GDL, i.e., these are the so-called "ink well pores", which influence the porosity of the GDL, but do not contribute to the permeability. It is also clear from Fig. 1 that the pore shape is not uniform. Such variations in the pore structure can cause two GDLs to appear similar in basic structural properties (i.e., porosity, mean pore size, etc.), yet have significantly different effective water vapor diffusivity values, as shown in a comparison of GDLs A and B in Table 3.

Finally, Datta and Rinker [52] provide the following correlation for the mean pore radius change from a dry to a wet porous medium

$$\frac{a}{a^0} = \left(\frac{\varepsilon}{\varepsilon^0}\right)^{1/3} = (1 - q_W)^{1/3} \tag{7}$$

The use of Eqs. (5)–(7) in Eqs. (2)–(4) results in correlations that describe the effect of the liquid loading on the DGM constants, and hence, on the effective gas-phase diffusivity.

Alternately, as is more common, one may empirically correlate effective diffusivity as follows [53]

$$D^e_{O_2,D} = \varepsilon^\beta D_{O_2,G} = \underbrace{\left(\varepsilon^0\right)^\beta D_{O_2,G}}_{D^{e,0}_{O_2,D}} (1 - q_W)^\beta = D^{e,0}_{O_2,D}(1 - q_W)^\beta \tag{8}$$

where $D^{e,0}_{O_2,D}$ is the effective diffusion coefficient of oxygen in a dry GDL, while $D_{O_2,G}$ is the gas-phase diffusivity of O_2. The exponent β is empirically fitted and of the order of 1.5–3 [53].

The data of Hwang and Weber [53] were measured from limiting current density of hydrogen in a specially designed cell. However, there are few data of this nature available in the literature measured directly for oxygen [54,56]. On the other hand, water vapor diffusivity, typically in a dry GDL, i.e., $D^{e,0}_{W,D}$, is more readily measured via a (steady-state) diffusion cell, as described by LaManna et al. [57], or via a transient diffusion technique described below, and may be used as a rough measure of the oxygen effective diffusivity to correlate with limiting current density, as follows.

For the same GDL, thus, from Eq. (8) used for O_2 as well as for water vapor, W

$$D^e_{O_2,D} = D^{e,0}_{W,D}\left(\frac{D_{O_2,G}}{D_{W,G}}\right)(1 - q_W)^\beta \tag{9}$$

In other words, the effective diffusivity of oxygen and that of water vapor are proportional for a given GDL under dry conditions. Consequently, Eq. (1) takes the form

$$i_{C,L} = \left\{\frac{4F}{RTL_D}\left(\frac{D_{O_2,G}}{D_{W,G}}\right)\right\} D^{e,0}_{W,D}(1 - q_W)^\beta p_{O_2} \tag{10}$$

where the term in the curly brackets is a constant. In other words, one would expect a linear relationship between the limiting current density and the effective water vapor diffusivity measured under dry conditions, or for a case when the liquid loading in the GDL is not high. However, for cells operating at high operating current densities or under wet conditions, one would expect deviations, as the GDL gradually becomes saturated with water. Results supporting these conclusions are provided in Section 3.2.

Table 3
A comparison of GDL structures with different effective water vapor diffusivities.

Property	GDL A	GDL B
Thickness (μm)	192	184
Basis weight (g m^{-2})	56.8	56.1
Porosity (%)	81.4	81.6
Total pore area (m^2 g^{-1})	9	9.3
Total pore volume (mL g^{-1})	2.5	2.6
Mean pore diameter (μm)	48.3	50.7
Predicted D_{eff}/D_0 (Bruggeman)	0.734	0.729
Measured D_{eff}/D_0 (water vapor)	0.135	0.241

3.1. Measurement of water vapor effective diffusivity

The effective water vapor diffusivity values provided in Table 3 were measured with a specially designed apparatus shown schematically in Fig. 4. This is a transient measurement device, where at time $t < 0$, the GDL and dry chamber have been completely purged of any water via bottled dry air. At time $t \geq 0$, a wet chamber with an RH of 100% is lowered onto the GDL sample, and an RH sensor is placed at a known distance from the bottom of the GDL sample, as shown in Fig. 5. The transient water vapor content at this location is measured as a function of time over 2 min, and used to determine the effective water vapor diffusivity of the GDL, D_{eff}, by fitting to the transient solution of a 1-D model based on Fick's second law

$$\frac{\partial c}{\partial t} = D_{eff}\frac{\partial^2 c}{\partial x^2} \quad \text{for} \quad (0 < x < L_s, \;\; t > 0) \tag{11}$$

$$\frac{\partial c}{\partial t} = D_0\frac{\partial^2 c}{\partial x^2} \quad \text{for} \quad (L_s < x < L, \;\; t > 0) \tag{12}$$

where c is the water vapor concentration, x is the distance along the sample path, L_s is the thickness of the GDL sample and L is the distance from the bottom of the GDL sample to the RH sensor, D_{eff} is the effective water vapor diffusion coefficient of the sample, and D_0 is the diffusion coefficient of water vapor in air. The D_0 value is adjusted for temperature and pressure of the room via the modified ideal gas law and the collision integral.

This model is solved subject to the following boundary conditions: 1) saturated water vapor at the wet chamber/GDL interface, 2) vapor flux is continuous at the GDL/Dry chamber interface, and 3) there is no mass flux out of the dry chamber (sealed chamber). The initial condition is no water vapor within the sample or dry chamber at the beginning of the test.

Further, the model involves four key assumptions: 1) there is no convection (pressure driven flow), 2) the gas density (T and P) is constant, 3) water vapor diffuses instantly across the diffusion barrier at the start of the test, and 4) there is no significant water condensation within the GDL during this test. While the first two assumptions are reasonable, and the third can be verified by measuring the diffusion curve of the film without a GDL sample present, the fourth assumption is more difficult to verify. Here it is

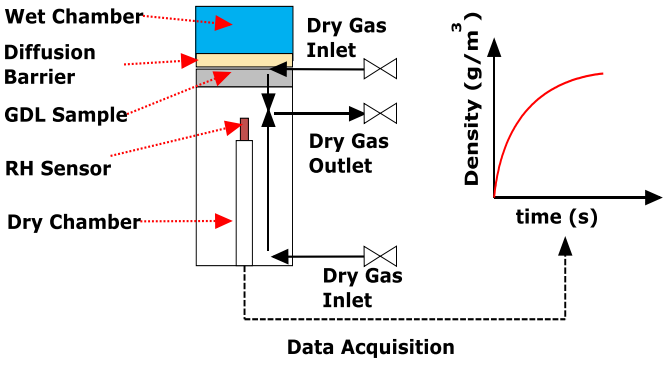

Fig. 4. Schematic of a transient water vapor diffusivity measurement tool.

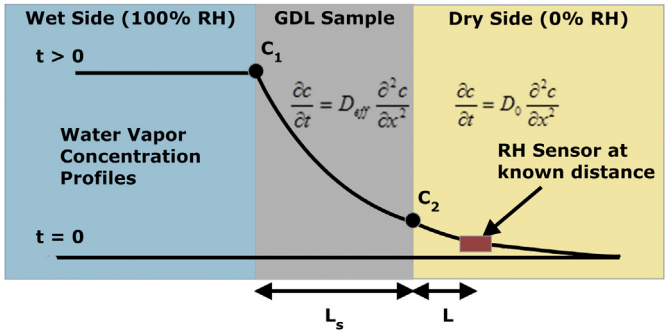

Fig. 5. Conceptual diagram of a transient water vapor diffusivity measurement apparatus.

assumed to be true by ensuring that both chambers are dry at $t \leq 0$, and holding the system at constant temperature during the test.

For any given continuous GDL roll, the diffusivity value is determined by measuring six different locations on the roll (three across the web at both the start and end of the roll), and then averaged.

It is, of course, possible to control the effective diffusivity of a continuously made paper GDL roll by altering the pore structure at the substrate and at the MPL levels (Fig. 1). The base substrate material can be altered either by modifying the fill matrix in the substrate or by changing key parameters in the manufacturing process to alter the pore structure. The PTFE content in the substrate can be modified to change the hydrophobicity level, which also directly impacts both the total porosity and the effective water vapor diffusivity of the GDL. The MPL structure can also be modified with different particle sizes and types, as well as PTFE loading. Based on an understanding of the impact of these modifications, it is possible to manufacture GDLs with specific effective diffusivity values for optimal cell performance under a given set of conditions.

3.2. Water vapor diffusivity and wet limiting current density

As argued above, the water vapor diffusivity hence measured is a good predictor of the GDL performance in a fuel cell and limiting current density. Thus, a group of GDL samples with different effective water vapor diffusivities was fabricated. The effective water vapor diffusivity in these samples was modified by altering the pore structure of the substrate, the PTFE content in the substrate, as well as the design and number of the MPLs coated on the surface.

The measured effective water diffusivity values correlate well with *in-situ* performance, as shown in Fig. 6. It is clear from this Fig. 6 that with increasing effective water vapor diffusivity, the mass transport "knee", along with the limiting current density, is extended to proportionately higher currents, as predicted by Eq. (10). The initial impact is significant when the diffusivity changes from a value of x to a value of $2x$, but the impact is reduced when progressing subsequently from a value of $2x$ to a value of $3x$. This indicates that there are other factors, e.g., higher GDL loading, q_W, at high current densities that limit performance once the effective water vapor diffusivity becomes very high. Further, it is evident from this Fig. 6 that the higher diffusivity not only impacts the limiting current, but also to some extent even the performance in the region removed from mass transfer limitations.

Additional GDL samples were fabricated and their wet limiting current densities were correlated directly to effective water vapor diffusivity, as rationalized in Eq. (10) and shown in Fig. 7. Although the data are limited, it is clear that there is a strong linear

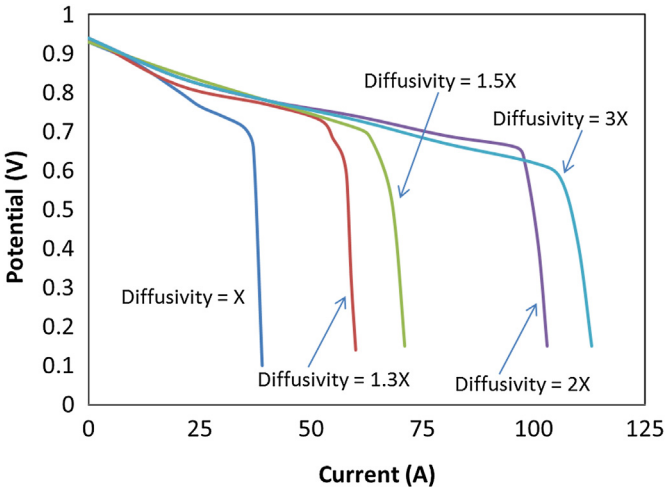

Fig. 6. Fuel cell performance for GDLs with different effective water vapor diffusivity values.

correlation ($R^2 > 0.95$) between effective water vapor diffusivity and wet limiting current densities, with the straight line seemingly passing through the origin. It should be noted that the range of these experiments is limited to effective diffusivity ratios (D_{eff}/D_0) > 0.2 under specific operating test conditions (70 °C, 12 psig, 2x stoichiometric flows, 100% RH A/C) and that the trend may well be nonlinear outside of these conditions, as indicated in Fig. 6, and rationalized via Eq. (10). Regardless, it is clear from both Figs. 6 and 7 that there is a direct relationship between the measured effective water vapor diffusivity and the ultimate cell performance. It is likely that the nonlinearity observed in Fig. 6 for very high water vapor effective diffusivity is because of increased water loading at high current densities. This could be confirmed by directly measuring oxygen effective diffusivity as a function of q_W, but such experiments have apparently not been performed as of yet. An effective oxygen diffusivity measurement tool that can be operated under various humidification levels could potentially predict cell performance more accurately than the standard dry diffusivity tool and should be developed. In summary, we may conclude for now that the readily measured water vapor effective diffusivity as described

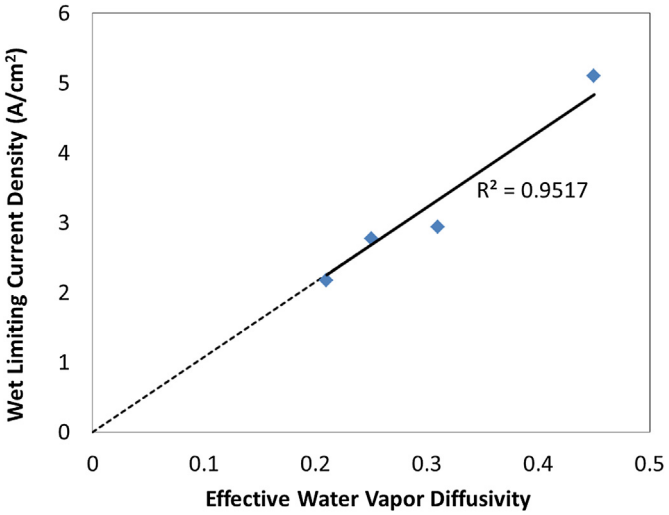

Fig. 7. Correlation of effective water vapor diffusivity measurements and wet limiting current density data (70 °C, 12 psig, 100% RH on A/C) for four GDL designs.

above can be used to reliably predict the performance of the GDL in a PEM fuel cell.

3.3. GDL air permeability

The air permeability of the GDL is typically measured in both through-plane and in-plane directions. The through-plane measurement is also indicative of the effective diffusion coefficient of oxygen through the GDL to the catalyst layer. Thus, the performance tends to improve as through-plane permeability increases. The in-plane measurement, on the other hand, is indicative of the convective flow of the reactant gases through the GDL, parallel to the flow channels of the bipolar plate. The impact of the GDL structure on these properties is understandably different. The air permeability of the GDL can be altered by changing the thickness, the compressibility, the porosity, the pore size, and the pore shape of the GDL.

The through-plane permeability of the GDL decreases as GDL thickness increases. This is, of course, because thicker GDLs have longer diffusion lengths, but the effect is also magnified during operation because thicker GDLs tend to retain more water, blocking pores available for diffusion. The in-plane permeability, on the other hand, tends to increase as GDL thickness increases, due to increased porosity of the thicker GDL (Table 2). Increased in-plane permeability is helpful for interdigitated flow field designs due to improved convection of the gases, but is undesirable for fuel cell stacks with parallel or serpentine flow field designs. Issues such as uneven flow sharing can then arise and allow for water buildup in the channels, resulting in reactant bypass [58], which reduces cell performance. On the other hand, convection through the GDL in an interdigitated bipolar plate reduces the effective through-plane diffusion path length.

The permeability of the GDLs can be measured by controlling the flow of gas (typically air or nitrogen) through the material in a specific direction. Since most GDLs have some compressibility, the permeability changes depending on the compression level [59]. One of the simplest ways to measure through-plane permeability is with a manual densometer, such as the one manufactured by Gurley Precision Instruments of Troy, New York, and described in detail in the literature [45]. This tool can also be used to measure in-plane permeability by placing a seal around the through-plane hole and recording the time for the fluid to permeate through the GDL sample.

4. The microporous layer (MPL)

The microporous layer (MPL) (Fig. 1) is typically comprised of carbon and graphite particles that are mixed with PTFE and some binder material into a coating ink for application. The MPL performs many roles in improving the GDL function, that include: 1) providing a smoother surface for contact with the catalyst layer/membrane, 2) providing appropriate pore size to aid in water removal/retention in the MEA, 3) preventing catalyst migration into the GDL substrate and hence losing contact with the membrane, and 4) enhancing electronic transport to the current collectors.

4.1. MPL characterization techniques

Pore shape and connectivity of the MPL can be measured via standard intrusion porosimetry, provided that the MPL can be coated on to a non-porous material, or alternately if the substrate porosimetry data can be separated from the GDL porosimetry data. The thermal properties of the MPL are measured via a standard method, such as laser flash analysis, while electrical resistivity is measured using the four probe method [45]. The surface roughness can be analyzed via a simple profilometer, or through a more in-depth approach, such as a laser confocal microscope, or an atomic force microscope. Compressibility of the MPL is measured via taking the thickness at multiple compressive loads, similar to the standard method for GDL substrates. Durability is tested via long-term testing (>500 h) to examine for MPL washout (the removal of loosely bound MPL particles by product water thereby reducing MPL loading), reduction in hydrophobicity, and MPL carbon corrosion. Adhesion to the GDL substrate is determined via a standard tape test, in which an adhesive tape is applied to the surface at a variety of controlled pressures and then removed and measuring the amount of material removed by the adhesive.

There are the following four key variables, discussed below, which can be altered in the MPL design: 1) number of MPLs, 2) MPL thickness, 3) particle size, and 4) particle type.

4.2. Effect of the number of MPLs

When the MPL was, rather recently, first applied to a GDL [60], the goal was to create a thin layer with very small hydrophobic pores that promote water transport away from the catalyst layer. Testing was limited to mainly small carbon black particles (e.g., Vulcan XC-72, Shawinigan) and little attention was paid to the quality of the coating. The modern MPLs are more sophisticated, and are designed to control the size of the pores gradually from the catalyst layer to the flow channel, as well as the distance that the MPL penetrates into the substrate, to avoid elimination of large pores in the substrate. The water transport can be greatly enhanced by generating a controlled pore structure with smaller pores near the catalyst layer, slowly moving to larger pores as it moves through the material towards the bipolar plate, as shown schematically in Fig. 8. The optimal design of the MPL structure is dependent on the application, the operating conditions, the flow field design, the type and quantity of catalyst, and the membrane used in the fuel cell. The desired MPL structure in Fig. 8 can be accomplished simply by applying two or more different MPLs to the GDL, where each MPL has a different level of hydrophobicity, particle size and type, and thickness.

The performance of a GDL with a single MPL is compared in Fig. 9 under the same operating conditions with that of the same substrate with two MPLs. The two-layer MPL clearly provides not only a higher limiting current density, but also enhances the performance throughout by reducing the Ohmic overpotential via improved protonic conductivity and interfacial contact, while extending the mass transport knee significantly, due to improve water transport properties. In fact, modern GDL structures can have as many as three MPLs added to the substrate. For most low power applications with minimal humidification levels, a single MPL will often suffice for meeting performance goals. For high power applications, or under very wet conditions, multiple MPLs may be

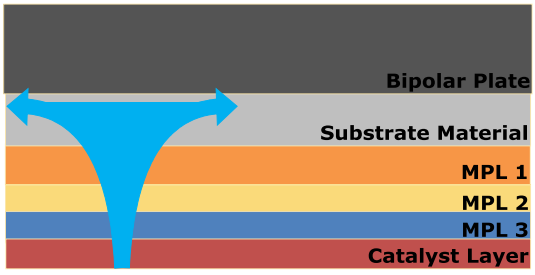

Fig. 8. Schematic of liquid water removal from the catalyst layer being facilitated from small pores in the outermost MPL to larger pores on the innermost MPL to the largest pores in the GDL substrate material.

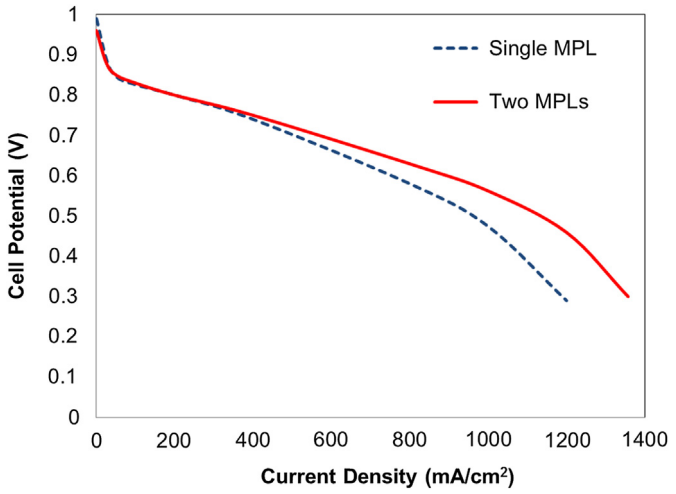

Fig. 9. Comparison of fuel cell performance with the same base GDL substrate coated with a single MPL and with 2 MPLs.

required to achieve the desired fuel cell performance. It is important to remember that although multiple MPLs provide additional control of the pore structure and enhanced performance, this comes at an additional manufacturing cost associated with the additional formulation and coating of these layers.

When designing a GDL, it is also important to recognize that the demands on the anode and the cathode are different. Altering the number and type of MPLs used can help to force the flow of product water in one direction or the other. This can be helpful in applications such as the direct methanol fuel cell (DMFC), where forcing product water from the cathode through the membrane to the anode may help reduce methanol crossover by diluting the reactants at the anode catalyst layer and thereby improving performance. A fuel cell stack that has a different design for the anode and cathode GDLs may have a higher performance under specific operating conditions, but will, of course, also come at a higher cost because of more complex processing in high-volume production. These factors should be weighed when optimizing GDLs for a specific application.

4.3. Effect of the MPL thickness/loading

There have been numerous investigations that have examined the effect of MPL composition and thickness under a single set of conditions [34–43,61], but few that have examined their impact under different operating conditions, which is, therefore, our focus here.

In the first study, thus, a total of three MPL loadings were examined (10, 30 and 60 g m^{-2}) with medium-sized, i.e., 17 μm, particles under both wet (>70% RH) and dry (<30% RH) operating conditions. In the second study, a total of three MPL particle sizes (5, 17, 55 μm) with an intermediate loading (30 g m^{-2}) were examined under both wet (>70%RH) and dry (<30% RH) conditions. In all of these studies, the same hydrophobicity level was used in the MPLs, and the MPLs were coated on the same base substrate material. The resulting GDL samples were tested in a 50 cm^2 single fuel cell, with double-pass serpentine flow channels on the anode and triple-pass serpentine channels on the cathode, operated at 70 °C and 12 psig back pressure, with both anode and cathode flows held at 2*x* stoichiometric flow.

The results with different MPL loadings are presented in Figs. 10 and 11, respectively, for dry and wet conditions. As can be seen from Fig. 10 for dry conditions, increasing the MPL loading from 10 g m^{-2} to 30 g m^{-2} improves performance significantly throughout. This is because the thicker MPL prevents the membrane from drying out, greatly improving the proton conductivity and thus reducing Ohmic losses. As the thickness is further increased to 60 g m^{-2}, however, the mass transport limitations in the GDL begin to dominate, as evident from the mass transport "knee" in Fig. 10. In general, it is important in designing a GDL to balance the improved conductivity associated with keeping the membrane adequately hydrated with transport limitations associated with flooding of the GDL with too much water.

On the other hand, as can be seen from Fig. 11, when the cell is operating under wet conditions, the performance improves as the thickness is reduced. There is little impact of loading in the Ohmic region as the membrane is well-hydrated because of operation at high RH, but the mass transport limitations are more pronounced with the higher MPL loadings. It is interesting to note, however, that the performance under wet conditions without an MPL has been shown to be worse [37], indicating that for this case, the optimal MPL loading is low, i.e., ≤10 g m^{-2}. Under very wet conditions, thus, it is important to keep the MPL loading low to prevent mass transport limitations due to flooding of the GDL.

4.4. Effect of the MPL particle size

The influence of MPL particle size, which determines the effective MPL pore size (Fig. 8), on fuel cell performance is described in Figs. 12 and 13, respectively, for dry and wet conditions. As can be seen from Fig. 12, under dry conditions, smallest particles in the MPL provide the lowest performance, while medium size particles provide the best. This is because the increased pore size allows improved membrane humidification and thus proton transport, reducing the Ohmic overpotential. As the particle size increases further, however, the pore size of the MPL tends toward pore size of the GDL substrate, which causes the performance to drop somewhat due to mass transport limitations, similar to a GDL without an MPL coating.

Under wet operating conditions, the largest particles show rapid mass transport loss as shown in Fig. 13, similar to what one would see using a GDL without an MPL. The mass transport limitations, and consequently the performance, improve significantly as the particle size is reduced to 17 μm. A further reduction in the particle size to 5 μm, while showing little effect of mass transport losses, causes an increase in the Ohmic overpotential due to overly

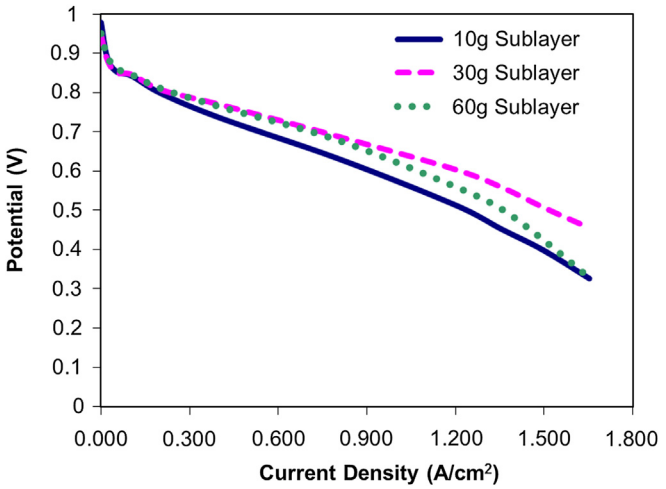

Fig. 10. Influence of MPL loading on fuel cell performance under dry operating conditions (<30% RH).

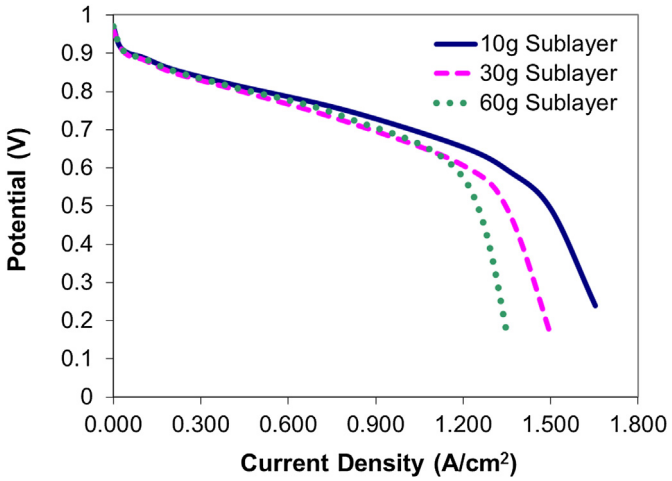

Fig. 11. Influence of MPL loading on fuel cell performance under wet operating conditions (>70% RH).

effective water removal. Overall, the medium particles, thus, perform the best under wet conditions in the tested range. In general, thus, a particle size between 5 and 20 μm should be used for applications under wet conditions. The optimal MPL design requires a balance between the Ohmic losses and the mass transport losses associated with different particle sizes.

4.5. Effect of the MPL particle type

In addition to thickness and particle size, the type of carbon particle can affect MPL performance. Classic MPL designs typically involved acetylene black [38], but other materials such as pelletized carbon blacks, metcokes, flake graphite, carbon nanotubes (CNTs), amorphous graphite, or synthetic graphite can be used in the MPL ink. The different types of particles can affect pore shape and connectivity, pore size, wettability, thermal and electrical properties, surface roughness, compressibility, durability (corrosion resistance), and adhesion to the GDL substrate. In addition, other materials, such as carbon fibers or even metallic particles [62], can be added to the GDL to improve performance for different operating conditions or applications. However, there is currently a lack of careful analysis in the literature on the effect of particle type in MPL.

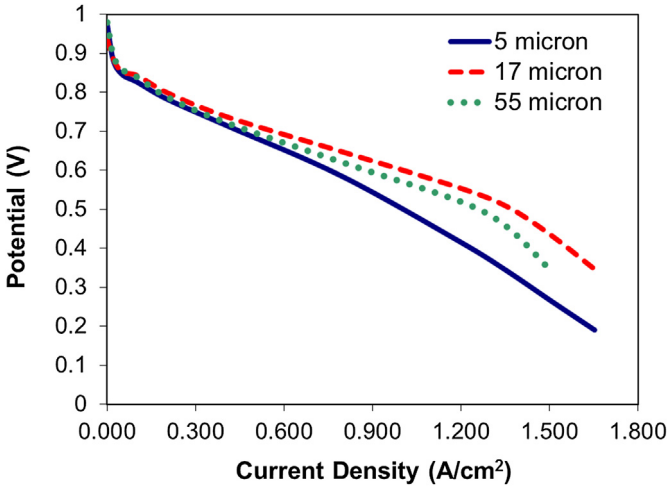

Fig. 12. Influence of MPL particle size on fuel cell performance under dry operating conditions (<30% RH).

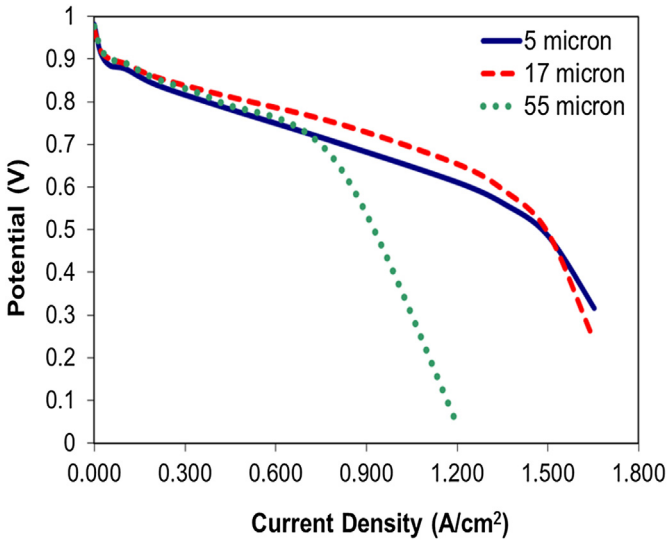

Fig. 13. Influence of MPL particle size on fuel cell performance under wet operating conditions (>70% RH).

Although different particle types can, thus, be used to improve the structural properties and functioning of the MPL, there are other practical considerations as well when selecting a particle type for an MPL. PEM fuel cells are especially susceptible to poisoning from very low levels of cations, especially from ferrous metals, so any MPL particle type used should be tested as a potential source of such contamination. In addition, the particles should be commercially available from more than one supplier, and of as low a cost as possible. Some particles, e.g., CNTs, while showing improved fuel cell performance, are unlikely to reach the required cost targets for commercialization. The selected particle type should also be compatible with standard MPL mix components such as PTFE and carbon black.

5. Conclusions

This paper discusses key GDL and MPL structural and design characteristics that determine the effectiveness of a GDL in meeting the disparate demands placed on it, namely, providing facile transport of reactants and products to and from the catalyst layer, efficiently conducting heat and electricity, and deftly managing membrane hydration, while providing structural protection to other delicate MEA components.

The key GDL structural properties including thickness, porosity, and pore size distribution. In general, thicker GDLs have higher porosity and larger median pore diameter, but also have longer diffusion path lengths and tend to flood more easily. The optimal GDL thickness is dependent on operating conditions, with thin GDLs preferred for high current density or very wet applications, and thick GDLs preferred on low current density or dry applications.

The correlation between effective oxygen diffusivity and effective water vapor diffusivity, which is more readily measured via transient method, and hence between effective water vapor diffusivity and the limiting current density is provided. It was found that the limiting current density and the cell performance improved rather proportionately with the measured effective water vapor diffusivity, until it reached a value where increasing GDL water loading becomes the limiting factor.

The MPL design is discussed at length, including the influence of MPL loading, MPL particle size, and MPL particle type. In general,

lower loadings and medium to small particle sizes are preferable under wet conditions owing to their effectiveness in water removal. Larger particles, medium thickness, and medium PTFE loadings are preferable under dry conditions to help keep the membrane adequately humidified for higher conductivity and lower Ohmic resistance. This work has also shown the benefit of applying multiple MPLs to a GDL, allow a more gradual change in pore structure, from very small pores near the catalyst surface to larger pores in the GDL substrate, to control the pore structure and enhance water management.

Designing a GDL while being mindful of these disparate considerations is clearly complex, requiring a careful balancing act.

Acknowledgments

We thank AvCarb Material Solutions of Lowell, MA, for providing the GDL samples, the use of the test equipment, and the funding to complete this work. We thank the DOE for providing partial funding for this work via Award Number: DE-FG36-08GO18051. We thank Michael Hickner and Alfonso Mendoza from the Pennsylvania State University for their assistance in collecting some images and data in support of this work.

Abbreviations

BOP	balance of plant
CCL	cathode catalyst layer
CCM	catalyst-coated membrane
DOE	Department of Energy
EERE	Energy Efficiency and Renewable Energy
GDL	gas diffusion layer
MPL	microporous layer
PEMFC	proton exchange membrane fuel cell
PTFE	polytetrafluoroethylene (teflon)
RH	relative humidity
SOFC	solid oxide fuel cell

References

[1] J.-H. Wee, Renewable Sustainable Energy Rev. 11 (2007) 1720–1738.
[2] http://www1.eere.energy.gov/hydrogenandfuelcells/pdfs/tiax_cost_analysis_pres.pdf.
[3] A.-J. Hung, C.-C. Yu, Y.-H. Chen, L.-Y. Sung, AIChE J. 54 (2008) 1798–1810.
[4] M. Kumar, S.J. Paddison, J. Mater. Res. 27 (2012) 1982–1991.
[5] J.X. Zhang, B.A. Litteer, F.D. Coms, R. Makharia, J. Electrochem. Soc. 159 (2012) F287–F293.
[6] H. Lee, T. Kim, W. Sim, S. Kim, B. Ahn, T. Lim, K. Park, Korean J. Chem. Eng. 28 (2011) 487–491.
[7] Y. Shao, R. Kou, J. Wang, V.V. Viswanathan, J.H. Kwak, J. Liu, Y. Wang, Y. Lin, J. Power Sources 185 (2008) 280–286.
[8] T.H. Yu, Y. Sha, W.G. Liu, B.V. Merinov, P. Shirvanian, W.A. Goddard, J. Am. Chem. Soc. 133 (2011) 19857–19863.
[9] C. Bas, L. Flandin, A.S. Danerol, E. Claude, E. Rossinot, N.D. Alberola, J. Appl. Polym. Sci. 117 (2010) 2121–2132.
[10] J. Stumper, S. Knights, E. Gyenge, J. Electrochem. Soc. 157 (2010) B425–B436.
[11] L. Kim, C.G. Chung, Y.W. Sung, J.S. Chung, in: T. Fuller, K. Shinohara, V. Ramani, P. Shirvanian, H. Uchida, S. Cleghorn, M. Inaba, S. Mitsushima, P. Strasser, H. Nakagawa, H.A. Gasteiger, T. Zawodzinski, C. Lamy (Eds.), Proton Exchange Membrane Fuel Cells 8, Pts 1 and 2, Electrochemical Society Inc., Pennington, 2008, pp. 945–953.
[12] L. Kim, C.G. Chung, Y.W. Sung, J.S. Chung, J. Power Sources 183 (2008) 524–532.
[13] J. Péron, Y. Nedellec, D.J. Jones, J. Rozière, J. Power Sources 185 (2008) 1209–1217.
[14] A.A. Franco, M. Gerard, J. Electrochem. Soc. 155 (2008) B367–B384.
[15] J.R. Davey, S. Sunde, R.L. Borup, ECS Trans. (2008) 1301–1311.
[16] N. Zamel, X. Li, Int. J. Hydrogen Energy 33 (2008) 1335–1344.
[17] H.S. Chu, C.P. Wang, W.C. Liao, W.M. Yan, J. Power Sources 159 (2006) 1071–1077.
[18] D. von Deak, D. Singh, E.J. Biddinger, J.C. King, B. Bayram, J.T. Miller, U.S. Ozkan, J. Catal. 285 (2012) 145–151.
[19] S. Ji, N. Myung, T. Kim, J. Mech. Sci. Technol. 25 (2011) 945–955.
[20] L. Magistri, A. Traverso, A.F. Massardo, R.K. Shah, 2005, 359–366.
[21] T.-P. Teng, Y.-H. Hung, T.-C. Teng, J.-H. Chen, Nanoscale Res. Lett. 6 (2011) 1–11.
[22] S. Kang, K. Min, S. Yu, Int. J. Hydrogen Energy 37 (2012) 5866–5875.
[23] K. Ramya, J. Sreenivas, K.S. Dhathathreyan, Int. J. Hydrogen Energy 36 (2011) 14866–14872.
[24] B.J. Kim, M.S. Kim, Int. J. Hydrogen Energy 37 (2012) 4290–4299.
[25] J.-K. Kuo, C.-F. Wang, Int. J. Hydrogen Energy 36 (2011) 11846–11855.
[26] Z. Xuancai, L. Xiao, S. Guoqiao, X. Dehong, IEEE Trans. Ind. Electron. 57 (2010) 1935–1944.
[27] W. Vielstich, A. Lamm, H.A. Gasteiger, Handbook of Fuel Cells: Fundamentals, Technology, and Applications, Wiley, Chichester, England; New York, 2003.
[28] T. Thampan, S. Malhotra, H. Tang, R. Datta, J. Electrochem. Soc. 147 (2000) 3242–3250.
[29] U. Pasaogullari, C.-Y. Wang, Electrochim. Acta 49 (2004) 4359–4369.
[30] P.M. Wilde, M. Mändle, M. Murata, N. Berg, Fuel Cells 4 (2004) 180–184.
[31] Z. Zhan, J. Xiao, D. Li, M. Pan, R. Yuan, J. Power Sources 160 (2006) 1041–1048.
[32] N. Parikh, J.S. Allen, R.S. Yassar, Fuel Cells 12 (2012) 382–390.
[33] R. Thiedmann, C. Hartnig, I. Manke, V. Schmidt, W. Lehnert, J. Electrochem. Soc. 156 (2009) B1339–B1347.
[34] H.K. Atiyeh, K. Karan, B. Peppley, A. Phoenix, E. Halliop, J. Pharoah, J. Power Sources 170 (2007) 111–121.
[35] J.T. Gostick, M.A. Ioannidis, M.W. Fowler, M.D. Pritzker, Electrochem. Commun. 11 (2009) 576–579.
[36] J.H. Nam, K.-J. Lee, G.-S. Hwang, C.-J. Kim, M. Kaviany, Int. J. Heat Mass Transfer 52 (2009) 2779–2791.
[37] A.Z. Weber, J. Newman, J. Electrochem. Soc. 152 (2005) A677–A688.
[38] E. Antolini, R.R. Passos, E.A. Ticianelli, J. Power Sources 109 (2002) 477–482.
[39] S. Park, J.-W. Lee, B.N. Popov, J. Power Sources 163 (2006) 357–363.
[40] S. Park, J.-W. Lee, B.N. Popov, J. Power Sources 177 (2008) 457–463.
[41] C.-J. Tseng, S.-K. Lo, Energy Convers. Manage. 51 (2010) 677–684.
[42] J.-H. Lin, W.-H. Chen, Y.-J. Su, T.-H. Ko, Energy Fuels 22 (2008) 1200–1203.
[43] Z. Fishman, A. Bazylak, J. Electrochem. Soc. 158 (2011) B846–B851.
[44] S. Park, J.-W. Lee, B.N. Popov, Int. J. Hydrogen Energy 37 (2012) 5850–5865.
[45] A. Arvay, E. Yli-Rantala, C.H. Liu, X.H. Peng, P. Koski, L. Cindrella, P. Kauranen, P.M. Wilde, A.M. Kannan, J. Power Sources 213 (2012) 317–337.
[46] R. Sousa Jr., E.R. Gonzalez, J. Power Sources 147 (2005) 32–45.
[47] J.J. Baschuk, X. Li, Int. J. Hydrogen Energy 35 (2010) 5095–5103.
[48] H. Wu, X. Li, P. Berg, Electrochim. Acta 54 (2009) 6913–6927.
[49] T. Thampan, S. Malhotra, J. Zhang, R. Datta, Catal. Today 67 (2001) 15–32.
[50] Z. Zhan, J. Xiao, Y. Zhang, M. Pan, R. Yuan, Int. J. Hydrogen Energy 32 (2007) 4443–4451.
[51] Y.M. Vol'fkovich, V.E. Sosenkin, N.F. Nikol'skaya, T.L. Kulova, Russ. J. Electrochem. 44 (2008) 278–285.
[52] R. Datta, R. Datta, R.G. Rinker, J. Catal. 95 (1985) 181–192.
[53] G. Hwang, A. Weber, J. Electrochem. Soc. 159 (2012) F683–F692.
[54] Z. Yu, R.N. Carter, J. Power Sources 195 (2010) 1079–1084.
[55] P.K. Das, X. Li, Z.-S. Liu, Appl. Energy 87 (2010) 2785–2796.
[56] C. Chan, N. Zamel, X. Li, J. Shen, Electrochim. Acta 65 (2012) 13–21.
[57] J.M. LaManna, S.G. Kandlikar, Int. J. Hydrogen Energy 36 (2011) 5021–5029.
[58] W. Sun, B.A. Peppley, K. Karan, J. Power Sources 144 (2005) 42–53.
[59] J.P. Feser, A.K. Prasad, S.G. Advani, J. Power Sources 162 (2006) 1226–1231.
[60] F. Lufrano, E. Passalacqua, G. Squadrito, A. Patti, L. Giorgi, J. Appl. Electrochem. 29 (1999) 445–448.
[61] C. Lin, T. Wang, F. Ye, Y. Fang, X. Wang, Electrochem. Commun. 10 (2008) 255–258.
[62] S.-Y. Huang, P. Ganesan, H.-Y. Jung, B.N. Popov, J. Power Sources 198 (2012) 23–29.